Impact of charge collection efficency and electronic noise on the performance of solid state 3D-microdetectors

J Prieto-Pena[1], F Gómez[1,2], C Guardiola[3], M C Jiménez-Ramos[4,5], J García López[4,5], A Baratto-Roldán[4,5], M Baselga[6], J Pardo-Montero[7] and C Fleta[8]

[1]Departamento de Física de Partículas, Universidade de Santiago de Compostela, 15782-Santiago de Compostela, Spain

[2]Grupo de Imagen Molecular, Instituto de Investigación Sanitaria, 15706-Santiago de Compostela, Spain

[3]Laboratoire de Physique des 2 infinis Irène Joliot-Curie (IJCLab-UMR9012) Université Paris-Saclay, Orsay, 91405 France

[4]Centro Nacional de Aceleradores, 41092 Sevilla, Spain

[5]Department of Atomic, Molecular and Nuclear Physics, Universidad de Sevilla, 41012 Sevilla, Spain

[6]ETP (KIT), Hermann-von-Helmholtz-Platz 1, 76344 Eggenstein-Leopoldshafen, Germany. Now at Deutsches Elektronen-Synchrotron DESY, Notkestrasse 85, 22607 Hamburg, Germany

[7]Grupo de Física Médica e Biomatemáticas, Instituto de Investigación Sanitaria, Santiago de Compostela, 15706 Spain.

[8]Instituto de Microelectrónica de Barcelona, Centro Nacional de Microelectrónica (IMB-CNM, CSIC), Bellaterra 08193 Spain

E-mail: `juan.prieto@usc.es`

Abstract. Microdosimetry has been traditionally performed through gaseous proportional counters, although in recent years different solid state microdosimeters have been proposed and constructed for this task. In this paper we analyze the response of solid state devices of micrometric size with no intrinsic gain developed by CNM-CSIC (Spain). There are two major aspects of the operation of these devices that affect the reconstruction of the probability distributions and momenta of stochastic quantities related to microdosimetry. For micrometric volumes the drift and diffusion of the charge carriers gives rise to a partial charge collection efficiency in the peripheral region of the depleted volume. Such effect produce a perturbation of the reconstructed pulse height (i.e. imparted energy) distributions with respect to the actual microdosimetric distributions. The relevance of this deviation depends on the size, geometry and operation conditions of the device. On the other hand, the electronic noise from the single event readout set-up poses a limit on the minimum detectable lineal energy when the microdosimeter size is reduced. This article addresses these issues to provide a framework on the physical constraints for the design and operation of solid state microdosimeters.

1. Introduction

High energy proton and heavier ion external beam therapy presents certain radiobiological and physical properties that allows better results than conventional photon and electron external radiotherapy in several types of cancer. Particle therapy is capable of inducing more damage to the tumor tissue at cellular and sub-cellular levels compared to photon therapy for comparable macroscopic dose levels and a better dose conformation to the target volume (Durante & Loeffler 2010). The rationale behind this behavior is that protons and ions can have a much higher Linear Energy Transfer (LET) than that produced by charged particles present in conventional photon and electron therapy, and this higher concentration of energy deposition leads to multiple clustered single-strand and double-strand breaks of cellular DNA. This amount of damage provokes a higher number of cell inactivation and apoptosis than with photon beams, since that damage is more difficult to repair (Brenner & Ward 1992). The increased number of facilities capable of providing these types of treatment has been increasing in the last years all around the world (Dosanjh, Amaldi, Mayer, Poetter et al. 2018, Particle Therapy Co-Operative Group 2019).

In particle therapy the dose is evaluated in terms of photon isoeffective dose, which is calculated as the product of the physical dose (absorbed dose to water) and the relative biological effectiveness or RBE (IAEA 2008). RBE is dependent on physical and biological factors, such as LET and several other biological processes that differ as a function of the target tissue (Britten, Peters & Murray 2001, Paganetti 2014). The Bragg peak, or the stopping range of the ions, coincides with the region of maximum RBE.

To characterize the photon isoeffective dose, it is important to know the energy deposition along the particle tracks at sub-micrometric levels (Krämer & Scholz 2000). As the traditional dosimetric quantities used in photon and electron external radiotherapy are based on average values of deposited energy in large regions and involving a large number of events, they cannot be used for the small scales needed in particle therapy. At microscopic scales, the stochastic nature of the radiation-matter interactions requires quantities based on distribution probabilities instead of metrics based on expectation values. The role of microdosimetry is to provide the full description of these quantities.

For microdosimetry applications, tissue equivalent gaseous proportional chambers (TEPC) are the most commonly used detectors. Their principle of operation is based on the use of a gas at a very low pressure with the same mass stopping power that a certain volume of tissue equivalent solid tissue, allowing to simulate a tissue equivalent microscopic site through the use of a gaseous macroscopic site. The main disadvantage of these detectors is that wall-effects can cause distortions in their reading. These effects can be avoided by using an iteration of the TEPC detectors called wall-less TEPC. Regardless, any model of TEPC will have millimetric spatial resolution due to its macroscopic size and show pile-up effects under beams of high fluence rate (as in

clinical beams, with fluence rates greater than 10^8 particles s^{-1} cm^{-2}). They are difficult to operate due to the use of high voltages, gas supply requirements and their size makes moving them a feat on its own. All these facts make them unfeasible for daily potential quality assurance and limit the practical use of these devices in clinical fixtures. Despite all these drawbacks, the TEPC technology has been the standard for microdosimetric measurements up to now, and recently, new versions of these detectors have been introduced, such as the mini-TEPC, which can improve most of the performance limitations associated with their size. (Colautti, Conte, Selva, Chiriotti, Pola, Bortot, Fazzi, Agosteo & Ciocca 2017, Farahmand, Bos, De Nardo & Van Eijk 2004, De Nardo, Cesari, Donà, Magrin, Colautti, Conte & Tornielli 2004, Kliauga 1990).

Solid state radiation detectors are commonly used to perform the dosimetric characterization of radiation fields, and present advantages such as fast response and good energy resolution. This family of detectors, having a higher mass density in the active volume than a gas-based detector, can be manufactured down to micrometric and submicrometric dimensions, and thus closer to the actual cell or cellular structure sizes of interest, allowing its use for microdosimetry applications. Not only can solid-state detectors have high energy resolution, fast signal processing and a small size, but they avoid some of the disadvantages of the TEPC, as they do not need high voltage bias and exhibit an overall easier device operation.

The use of three-dimensional architecture was proposed for silicon detectors (Parker, Kenney & Segal 1997) in the fields of medical imaging and particle tracking in high energy physics (Pellegrini, Lozano, Ullan, Bates, Fleta & Pennicard 2008). This configuration would be able to reduce the loss of charge carriers due to trapping effect and shorten the charge collection time compared to traditional planar solid-state detectors. In the 3D configuration, the voltage required to provoke full depletion in the bulk is also reduced, and for thin devices of up to 50 μm thickness the capacitance of a 3D micro-structured solid-state detector is at least two orders of magnitude lower than for traditional planar detectors (Pellegrini, Garcia, Balbuena, Cabruja, Lozano, Orava & Ullan 2009). The signal to noise ratio (SNR) is improved since SNR is inversely proportional to the capacitance (Spieler 2005).

Nevertheless, solid state devices also have some problems of their own that limit their usefulness in dosimetry. In the case of silicon, its non equivalence to tissue both in mass energy absorption coefficient and stopping power coefficient makes it necessary to apply correction factors in order to obtain the microdosimetric distributions in water. It is important that the type of devices described in this article are aligned with its sensitive volume perpendicular to the propagation direction of the beam, as a misalignment can produce a different mean chord length of the beam particles, affecting the reconstructed lineal energy spectra (Bolst, Guatelli, Tran & Rosenfeld 2018). Also, silicon devices are susceptible to radiation damage which degrades their performance with total dose. Additionally, there can be a loss of collected charge produced from the track ionization due to recombination that affects the reconstruction of the imparted energy distributions, thus modifying the microdosimetric spectra. This effect is summarized

usually through the charge collection efficiency dependence on the track impact position. Even though new developments in low-gain avalanche diodes (LGAD) use intrinsic amplification to enhance SNR (Pellegrini, Fernández-Martínez, Baselga, Fleta, Flores, Greco, Hidalgo, Mandić, Kramberger, Quirion et al. 2014), this amplification is still limited and the lack of intrinsic amplification in current 3D silicon detector technology compromises the signal to noise ratio for devices in the micrometer and sub-micrometer dimensions.

In this paper the active volume and charge collection properties of a cylindrical silicon microdosimeter developed by IMB-CNM (CSIC, Spain) was studied. In the case of the device employed for this work, the output signal is considered proportional to the imparted energy in the sensitive volume. From the spectra given by the detector signal, other microdosimetric quantities can be calculated. To evaluate the charge collection properties of the device, a model for charge collection efficiency as a function of the distance to the center of the active area was developed and then compared with experimental data from test runs conducted at the synchrotron of the Fondazione CNAO (Pavia, Italy) using a carbon ion beam and at CNA (Seville, Spain) using a proton microbeam. Additionally, the detection limit of 3D microstructured detectors as a function of their size is studied by means of a simple model that takes into account electronic noise from the readout electronics.

2. Materials and methods

2.1. Silicon microdosimeter

The microdosimeter employed in this work is a new type of three dimensional diode designed and developed by IMB-CNM (CSIC) at their facilities in Barcelona, Spain (Guardiola, Quirion, Pellegrini, Fleta, Esteban, Cortés-Giraldo, Gómez, Solberg, Carabe & Lozano 2015). The detector is comprised of several individual sensors or unit cells arranged in an array capable of individual readout for the detection of energy deposition events. These cells have a three-dimensional cylindrical structure etched inside the silicon bulk with an implanted p+ charge collecting electrode surrounded by a concentric n+ electrode trench. The cylindrical cell axis is perpendicular to the silicon wafer plane. A scanning electron microscope image and a schematic cross section of the device can be seen in figure 1.

Although the fabrication process allows the production of detectors with different diameter for the cylindrical sensors, in the device employed in this work we have set the the physical size of the silicon cylinder as 20 μm in diameter but due to the electric field distribution of the device the sensitive size of the cylinder is 15 μm in diameter. In this way the size and shape of the silicon sensitive volume is similar to those of mammalian cell (Ginzberg, Kafri & Kirschner 2015). The diameter of the central implanted electrode is 4 μm and the width of the n+ trench is 3 μm.

The sensors in the silicon die are arranged in a square matrix with p-electrode

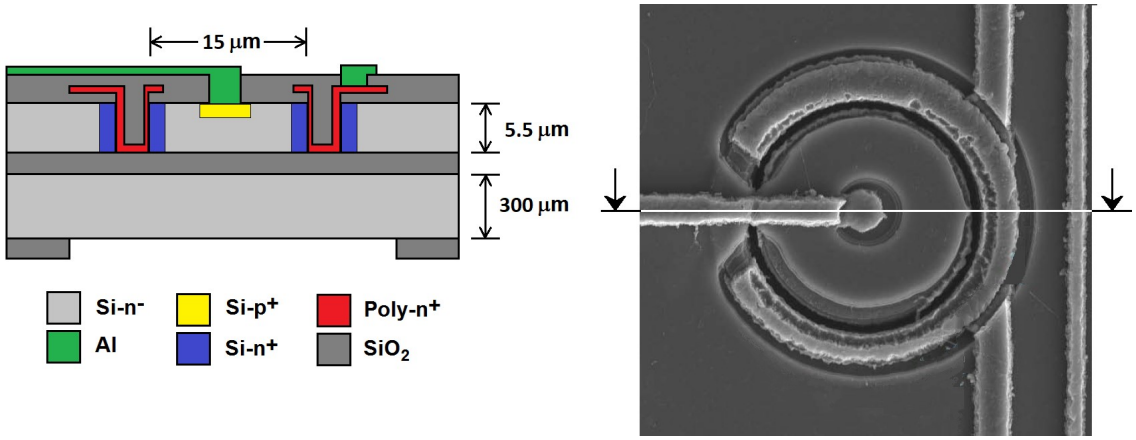

Figure 1. Cross section schematic of the detector (not to scale, left) along with an electron microscope image of the 3D-microdetector top-view (right).

individual readout. The pitch between two consecutive detector centers in this particular device is 200 μm although this can also be varied if desired. All the n-electrodes are connected to the same pad on the opposite side of the array for bias connection. In this work, only the readout from one individual cell at a time was fully instrumented, keeping the rest of the sensors grounded. The thickness of the sensitive volume is 5.5±0.5 μm. The energy resolution was estimated from measurements as 12% full-width at half-maximum (FWHM) at 660 keV. More information about the fabrication process and Technological Computed Assist Design (TCAD) simulations of the depletion volume and charge collection can be found at (Fleta, Esteban, Baselga, Quirion, Pellegrini, Guardiola, Cortés-Giraldo, López, Ramos, Gómez et al. 2015).

These detectors are designed to perform microdosimetric measurement at nominal fluence rate in hadrontherapy, allowing an instrumental verification of the lineal energy spectra at different depth and positions in a phantom (Gómez, Fleta, Esteban, Quirion, Pellegrini, Lozano, Prezado, Dos Santos, Guardiola, Montarou et al. 2016, Prieto-Pena, Gómez, Fleta, Guardiola, Pellegrini, Donetti, Giordanengo, González-Castaño & Pardo-Montero 2019). Their design produces a high conformation of the depleted region to a volume of approximately 900 μm^3. The intrinsic field gradients present in the device together with the charge drift and diffusion provoke that in the microdosimeter cell periphery the charge collection efficiency exhibits a relatively fast decay to zero values. Partially depleted silicon volumes present in the device lead to recombination of the ionization charge and partial charge collection. Due to the intrinsic technological limits in the microelectronics manufacturing processes, this charge collection transition is not negligible in general terms and can affect the reconstructed microdosimetric spectrum from the silicon micro-cell. This issue has been addressed in the present study to evaluate its significance and the limitation it poses for actual microdosimeter geometries. All the results presented in this work are shown in terms of energy deposition in silicon. However,the silicon energy deposition spectra can be converted to tissue equivalent material by a look up table methodology like that used in (Prieto-Pena et al. 2019).

2.2. Electrical simulations

Electrical simulations were conducted with a TCAD software, Sentaurus Synopsys. This software solves the Poisson equation for the studied geometry. TCAD simulations give a detailed description of the electrical field of the microdosimeter as well as the transient of a heavy ion through any angle of the device, giving the charge collection. The simulated device is a 20 μm diameter n-type (with a doping concentration of 8.61×10^{11} cm^{-3}) microdosimeter. The silicon wafers which the silicon detectors are fabricated from have a thickness of 5.5 $\pm$ 0.5 μm, with the thickness of this detector sample determined to be 5.3 μm. The silicon dioxide charge surface density used is 10^{11} cm^{-2}. The electrical simulations were carried out with 0 V, 5 V and 10 V bias voltage. Experimental measurements with 5 MeV alpha particles indicate a full depletion of the microdosimeter sensitive volume at a 5 V bias voltage (Fleta et al. 2015). The transient simulations use the HevyIon software function, with particles that have an LET$_f$ in silicon (Linear Energy Transfer function) of 1.282 10^{-5} pC/μm impinging perpendicularly to the surface of the microdosimeter.

2.3. Experimental set-up

The characterization of these devices with ion therapy beams were performed using a 115.25 MeV A^{-1} ^{12}C ion beam at Fondazione CNAO (Pavia, Italy). This synchrotron facility has an active scanning proton and carbon ion beam. During the measurements we used the signal from a mono-energetic pencil beam crossing 20 cm of air between the nozzle exit and the measuring instrument. Several measurements were carried out placing the microdosimeter behind a variable depth of polymethyl methacrylate (PMMA, density 1.186 g cm^{-3}). The depth was controlled using a motorized remote wedge system. The wedge system is formed by two 10° PMMA wedges allowing a variable depth of 3 mm to 40 mm with an uncertainty of the depth of approximately 30 μm. PMMA is a tissue-equivalent material, allowing to perform measurements in the fields of microdosimetry and radiobiology, the main scope of these detectors. The set of microdosimetric spectra obtained cover from the beam entrance plateau up to the Bragg peak for the ion beam used.

The microdosimeter was connected to a CAEN A1422H Hybrid charge sensitive preamplifier and to a CAEN N968 spectroscopy shaping amplifier. Then, the resulting pulse height was digitized through an Amptek MCA8000D multichannel analyzer placed in the experimental room, connected via Ethernet to a computer in the control room where the spectra were stored.

The previous work done using the CNAO clinical beam ^{12}C ion beam of CNAO with the cylindrical microdosimeters (Prieto-Pena et al. 2019) exhibit a reasonable agreement with the Monte Carlo simulations. Nevertheless, experimental pulse height distributions (using any bias voltage in the range of 0-20 V) always show a relevant tail with high number of counts in the low-energy part of the spectra and a small shift when compared with respect to the peak position in the simulated imparted energy distributions, as can

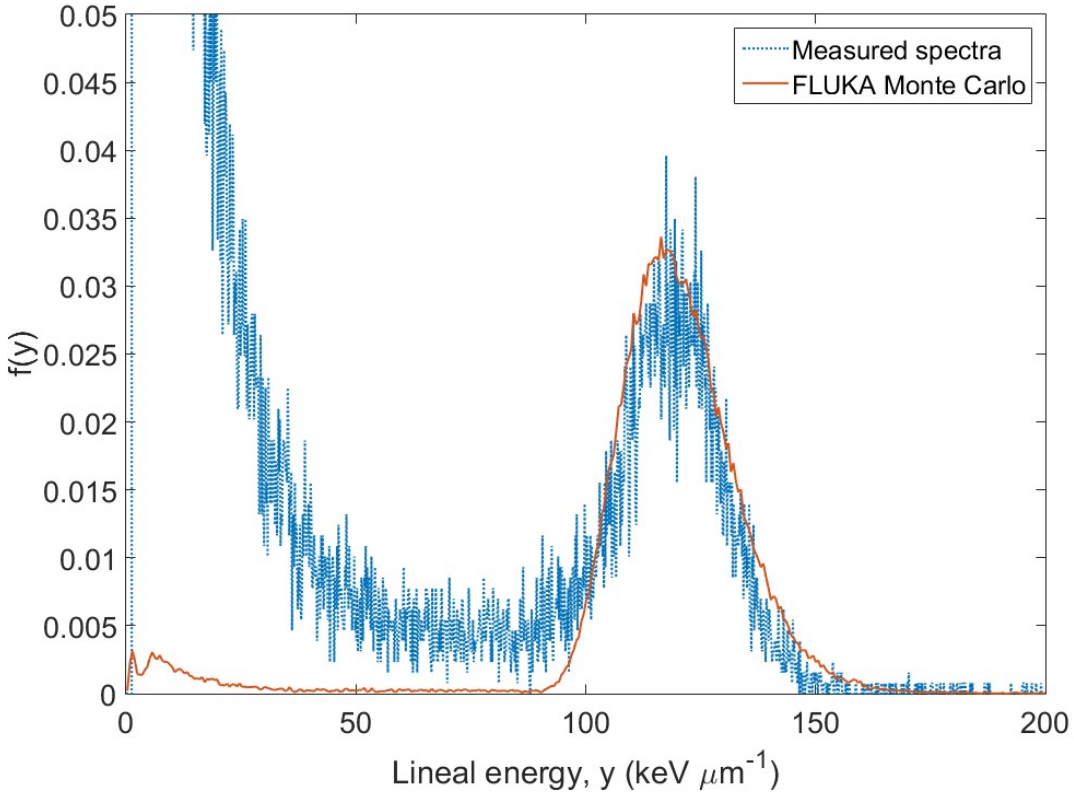

Figure 2. Experimental spectrum (blue dotted line) measured with the IMB 3D microdetector and FLUKA Monte Carlo simulation (red solid line) for 115.25 MeV A^{-1} ^{12}C ions traversing 25.20 mm of PMMA (Prieto-Pena et al. 2019).

be seen in figure 2, taken with no bias voltage. Electronic noise contributions, amplifier baseline shifts or pile-up events have not been found to be able to generate this distortion of the measured data from the microdosimeters.

The effect of spectrometry distortion in silicon microsensors has been reported previously in different devices with high granularity readout (Gimenez, Ballabriga, Campbell, Horswell, Llopart, Marchal, Sawhney, Tartoni & Turecek 2011, Campbell, Heijne, Holý, Idárraga, Jakubek, Lebel, Leroy, Llopart, Pospísil, Tlustos & Vykydal 2008). It is hypothesized that this behavior is produced by intrinsic field gradients and charge diffusion that modify the recorded spectra by the microsensor, provoking partially depleted volumes leading to recombination and partial charge collection in the periphery of the microcylinder.

2.4. Monte Carlo simulations

The experimental work was benchmarked against a Monte Carlo simulation of the beam energy deposition in an individual cell of the detector. Monte Carlo simulations were performed using the FLUKA Monte Carlo code (Ferrari, Sala, Fasso

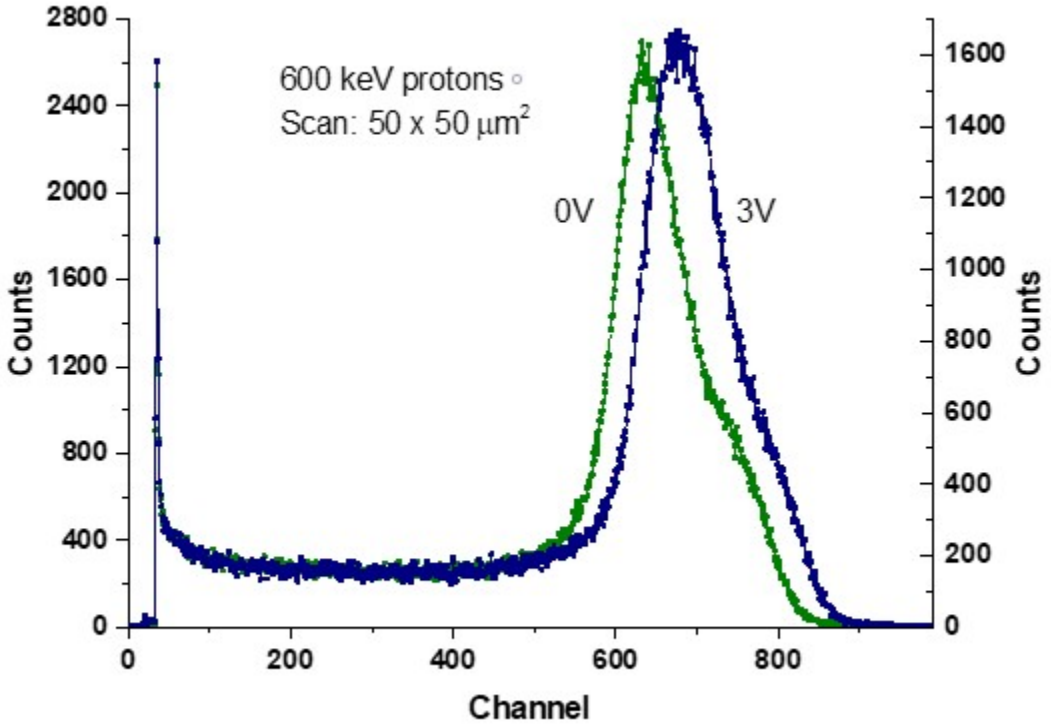

Figure 3. Pulse height spectrum for 600 keV proton beam in vacuum taken at the IBIC beam at CNA (Seville, Spain).

& Ranft 2005, Böhlen, Cerutti, Chin, Fassò, Ferrari, Ortega, Mairani, Sala, Smirnov & Vlachoudis 2014), developed by CERN and INFN.

There is a predefined configuration in the code for its use in hadrontherapy ("HADROTHErapy") that was selected for the simulations, changing the default thresholds for the transport of all particles, multiple scattering and delta ray production and corrections to form factor for Compton Scattering. A stricter additional limit to the kinetic energy threshold was selected, changing it to 1 keV. This option was selected to reproduce the experimental results more accurately without adding too much additional computation time, as detailed in (Böhlen, Cerutti, Dosanjh, Ferrari, Gudowska, Mairani & Quesada 2010).

For each geometry a simulation with 10^5 histories was computed. The estimated relative statistical uncertainty for the simulation in the plateau region of the Bragg curve is less than 2%. The code was commissioned against a water depth dose distribution of the same CNAO experimental beam measured with a Peakfinder variable water column and a PTW 34080 Bragg-peak chamber, similar to a procedure described elsewhere (Gómez et al. 2016). The simulation resembles the pencil beam's main characteristics, such as energy and angular spread at the exit window of the gantry together with

the transport across the PMMA wedge and mylar window and other materials of the detector metallic case and silicon support.

2.5. Charge Collection Efficiency model

The reconstructed imparted energy in the detector active volume is obtained from the pulse height distribution of the sensor. Each event pulse height is here considered as the convolution of the actual energy deposition along the silicon detector with the effective charge collection efficiency map. For the detailed evaluation of the Charge Collection Efficiency (CCE) we used the Ion Beam Induced Charge (IBIC) technique proton microbeam facility at CNA (Seville). During the irradiation the beam was scanned through the detector and the readout was performed through a synchronized amplifier and digitizer chain. The kinetic energy of the proton beam employed was 600 keV in different test runs conducted in vacuum. Figure 3 shows the pulse height spectra for 0 V and 3 V bias voltage in the IBIC proton beam.

A phenomenological model of the CCE was developed to describe the experimental results and Monte Carlo simulations. Here, not only the imparted energy was recorded, but also the position and director cosines of the trajectory of the particles when they enter into the detector volume. Ionization was generated in a 0.05 μm step voxel geometry, according to FLUKA distributions, along the straight line traversing the detector volume with an angle equal to the cosines of the particle. It was considered that for the particles and energy used the lateral straggling was negligible when compared with the dimensions of the detector (Berger, Coursey, Zucker, Chang et al. 1998). Once the ionization cloud along the track is produced, each charge voxel is weighted with the point dependent model CCE function, and then all the weighted charge contributions are eventually added to obtain the expected signal of each event.

The CCE function constructed is based on exponential functions with dependence on both the distance to the central axis of the cylinder (r) and the depth traversed by the particle (h). Radial and vertical dependence are separated in the model. A six-parameter function was constructed as shown in the following equation:

$$F(r,h) = f(r) \otimes g(h) \tag{1}$$

$$f(r) = \left[\frac{1+e^{-g_r r_1}}{1-e^{-g_r r_2}}\right]\left[\frac{1-e^{g_r(r-r_2)}}{1+e^{g_r(r-r_1)}}\right] \tag{2}$$

$$g(h) = \left[\frac{1+e^{-g_h h_1}}{1-e^{-g_h h_2}}\right]\left[\frac{1-e^{g_h(h-h_2)}}{1+e^{g_h(h-h_1)}}\right] \tag{3}$$

where r and h are the values of the radius and height (from the geometrical centre of the cylinder), r_1 and h_1 are the points in which the CCE function reaches a value of 0.5, r_2 and h_2 are the points in which the function goes to zero, and g_r and g_z are the gradients of the exponential decay. Additionally, the vertical h component has a hard limit in h=2.75 μm due to the detector dimensions (thickness of 5.5 μm).

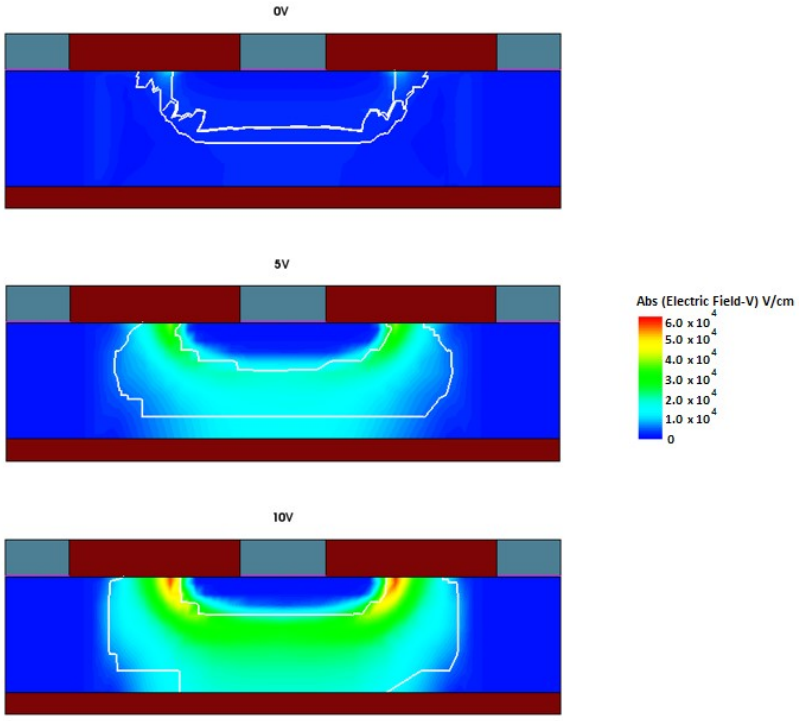

Figure 4. Electric field simulation using Sentaurus TCAD inside a microcylinder with a diameter of 20 μm and a thickness of 5.3 μm for biasing potential of 0 V (top), 5 V (center) and 10 V (bottom). The white line denotes the depletion volume inside the semiconductor.

3. Results

3.1. Charge Collection Efficiency

Figure 4 shows the electric field simulations inside a unit cell of the detector for different biasing potentials using TCAD simulations. The sensor lenticular shape depletion volume is shown in this figure delimited by the white solid lines. The simulations additionally reproduce the transient electric signal associated to the particle ionization event. For that scope, taking into account the 3D depletion volume that depends on the electric field inside the device, the drift and diffusion of charge carriers were simulated leading to the charge signal induction for the 3 μs shaping time of the electronic readout. Charge collection efficiency (CCE) was studied varying the particle track impact position within the geometry of the microdosimeter.

To verify the expected CCE predicted by TCAD simulations of the fabricated detector, IBIC experiments were performed at the CNA facilities in Seville, Spain, with protons of 600 keV kinetic energy and with the device fully depleted at a bias voltage of 5 V. The beam had a FWHM varying from 3.46 μm (X) up to 4.85 μm (Y). In those tests, the beam position was scanned following a two-dimensional grid while the detector collected charge in each energy deposition event was recorded. Normalized data is shown

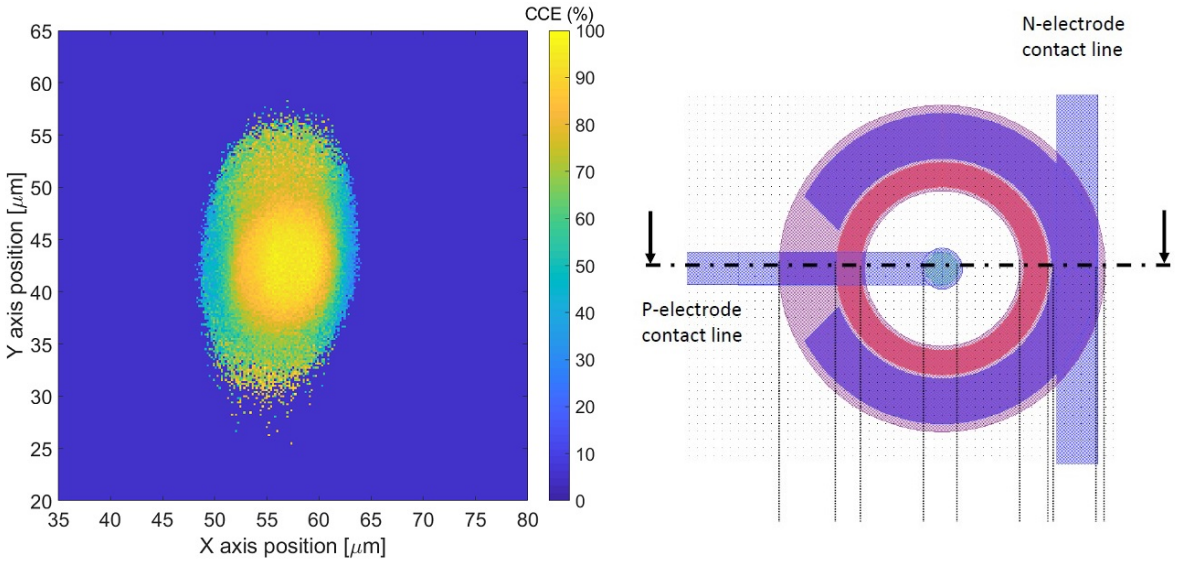

Figure 5. Normalized charge collection map recorded at the IBIC test performed at CNA (Seville, Spain) with the IMB 3D Cylindrical Microdosimeters. Legend shows the charge collection percentage normalized to the central values calculated for each pixel as a function of the beam position. The irregular shape of the map is due to the different dimensions of the proton beam along the X (FWHM 3.46 μm) and Y axis (FWHM 4.85 μm). On the right side there is a top view sketch of the IMB 3D microdetector from (Fleta et al. 2015) to compare with the IBIC heat map.

in figure 5. The CCE was calculated by normalizing the energy deposition values to the most probable energy deposition of the proton beam in the 5.5 μm silicon layer of the sensor. It can be seen that most of the events apparently deposit less energy into the volume than expected, with a strong dependence on the position. Events with low charge collection efficiency occur in the periphery of the cylinder, whereas events with high CCE are more aggregated into the microsensor central region. These numerical results from the microbeam measurements and the CCE model are compared in next section. The experimental results shown in figure 5 show additional effects due to the lack of symmetry of CCE with respect to the cylindrical sensor axes that can be explained due to the different beam FWHM along those axes.

3.1.1. Charge Collection Efficiency model The values of the model parameters were assessed with the help of the IBIC test, with the gradients obtained by a χ^2 minimization between the ^{12}C experimental data and the Monte Carlo smeared spectra, and its results

Table 1. Table showing the CCE parameter values for the model.

r_1	r_2	g_r	h_1	h_2	g_h
7.2 μm	20 μm	3.1 μm^{-1}	2.75 μm	10 μm	5.75 μm^{-1}

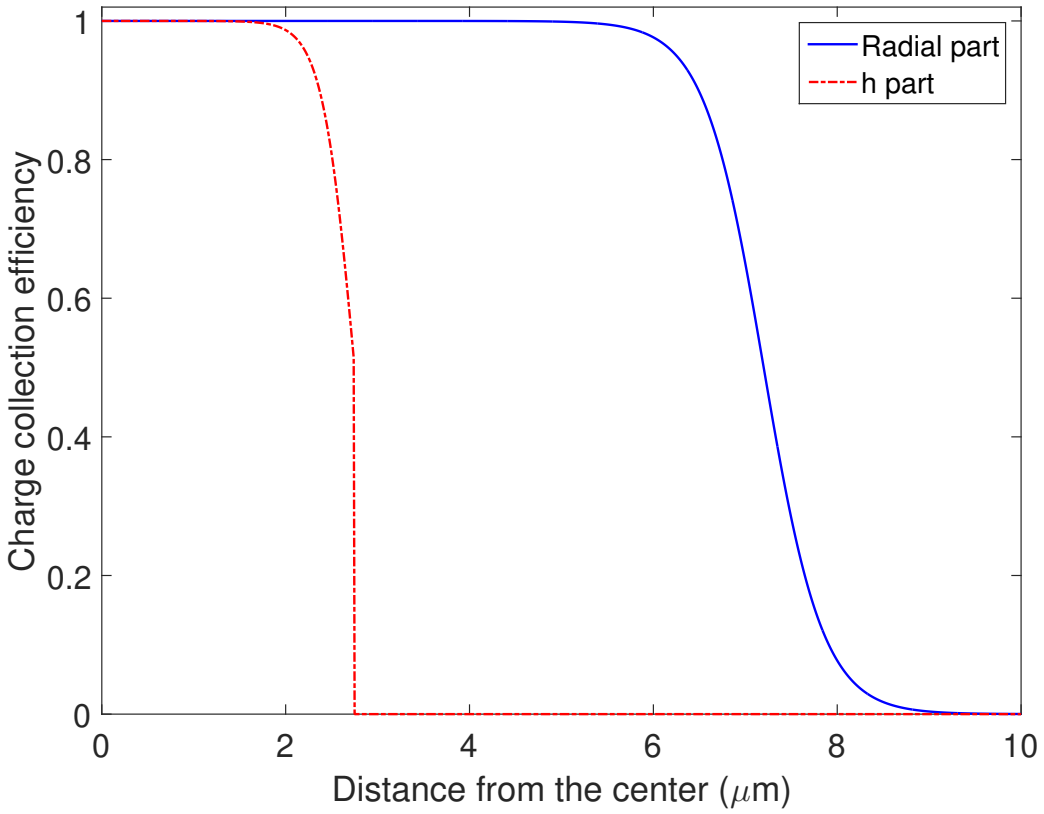

Figure 6. Graphic showing the behavior of the two components of the CCE model with the parameters of table 1. All distances are from the geometrical center of a 15 μm diameter and 5.5 μm height cylinder.

are shown in table 1. Figure 6 shows the components of the charge collection efficiency model and its values as a function of the distance to the geometrical center of the detector.

The model parametrization was compared with both the TCAD simulations and experimental results from the IBIC test with proton ions at CNA. Figure 7 shows the comparison between the analytical model and the TCAD simulation whereas figure 8 shows the comparison between our model and the IBIC experimental results. In the comparison with the IBIC beam its width was taken into account through a convolution between a Gaussian distribution with $\sigma = 2$ μm and the analytical CCE model.

TCAD simulations shown in figure 7 have a significant agreement with the analytical model for distances bigger than $r = 2$ μm, whereas for smaller distances the TCAD simulation shows a relative difference of up to 12 % compared with the summarized model. This difference cannot be confirmed experimentally due to the limited sensitivity of the experimental data to the detailed actual charge collection behavior in the silicon microcylinder.

The model was then used to modify the response of the energy deposition along

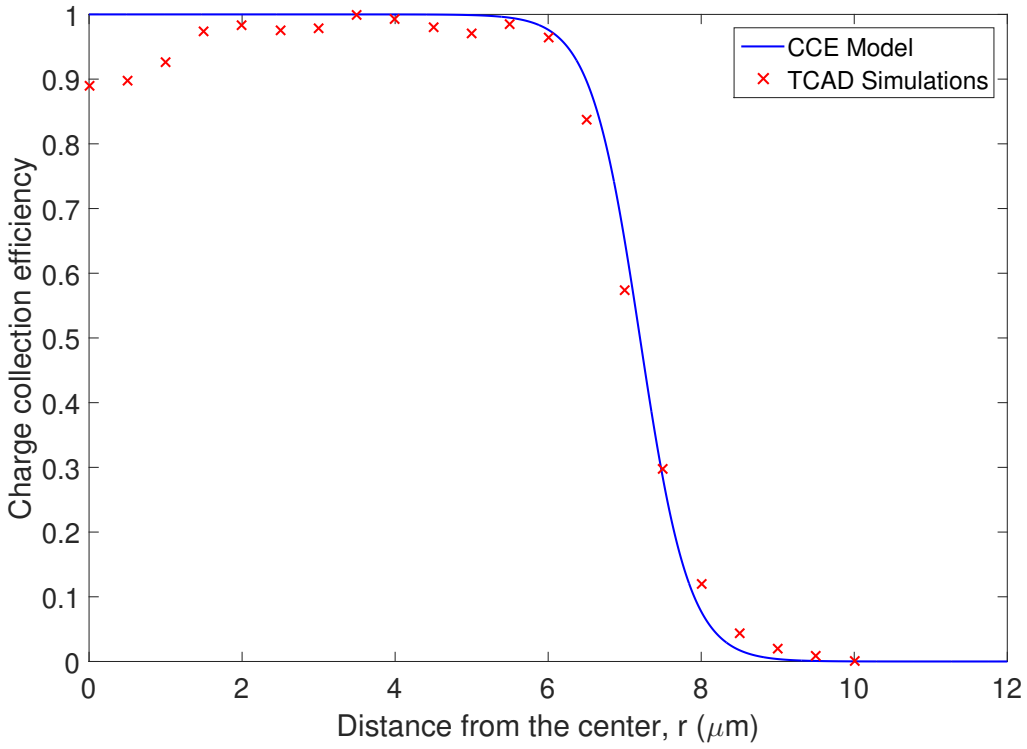

Figure 7. Comparison between the charge collection efficiency predicted from our model and from TCAD simulations results.

the ionizing particle tracks using the Monte Carlo simulations. Results for lineal energy in silicon are shown for several depths along the Bragg curve in figure 9. The smearing process causes a shift of the peak position when compared with the un-smeared Monte Carlo spectra, which varies in value all along the Bragg curve, together with the appearance of a low pulse height tail due to events associated to low CCE regions in the sensitive volume. The lineal energy distribution peak shift was found to be proportional to the LET of the particles at each depth. After this correction was applied to the experimental spectra obtained in the CNAO experiment the smeared Monte Carlo and the experimental results agree significantly and the peak position discrepancy shown in figure 2 is corrected.

The peak shift corrections are proportional to lineal energy for all measured depths with the cylindrical microsensor up to the Bragg peak, as shown in figure 10. The shift linear behavior along the Bragg curve represents approximately a relative correction of 6%. The uncertainties for all points in the figure are less than 5% (k=2). It remains unclear if this proportionality holds true for the low lineal energy region and more experiments with protons or other ion beams should be conducted to further understand the phenomena.

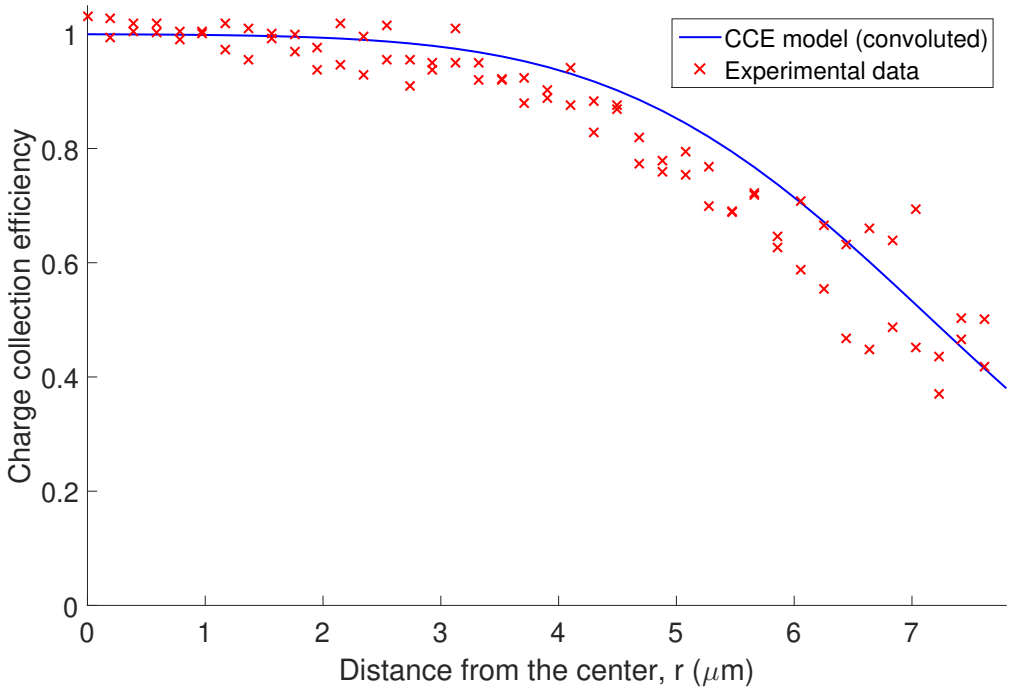

Figure 8. Comparison between charge collection efficiency results from the experimental test at CNA and from a convolution between a Gaussian distribution with $\sigma = 2\mu$m to take into account the finite width of the proton beam that contributes to smear the experimental CCE distribution.

3.2. The detectability problem

One of the main scopes in microdosimetry is the measurement of microdosimetric distributions at micrometric and submicrometric scales. In the case of submicron equivalent mass thickness devices, they would be sensitive to the track structure and charge cluster distributions in the material.

As we have seen previously, the fidelity of reconstruction of microdosimetric spectra can be seriously compromised especially in the low lineal energy region by effects related to CCE in the small volume of the solid state microdosimeter. On the other hand, as current devices have no intrinsic gain, there is additionally a physical limitation on the threshold of detection for low lineal energy. Although many possible designs are feasible, in terms of simplicity we have considered here a cylindrical geometry where the cylinder diameter and its height are equal to a given dimension L. In the previous section of the paper we have dealt with an diameter to height ratio of 15 μm / 5.5 μm of almost three. Although this change of geometry would yield different values of capacitance and leakage current, for a given sensor design the obtained detection limits will not be changed more than 5%, considering that the dimension of interest in this case is the thickness of 5.5 μm. In all this section we express the lineal energy in silicon. In order to convert it to tissue equivalent values there are several different approaches, but as an approximate

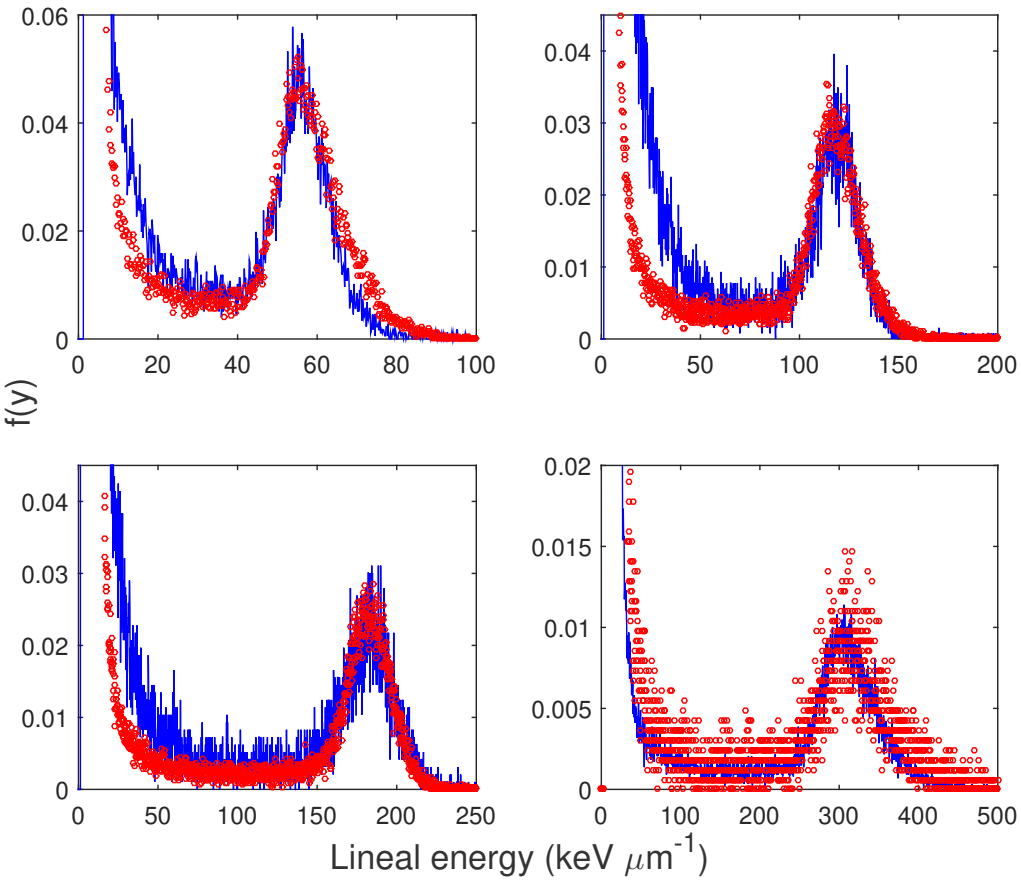

Figure 9. Comparison between the Monte Carlo spectra after applying the charge collection of the device and the experimental spectra. From left to right and top to bottom: 12.20, 25.20, 27.20 and 28.125 mm PMMA. Blue lines indicate smeared FLUKA Monte Carlo simulations, while red circles indicate the CNAO experimental measurements.

conversion a geometrical scaling factor 0.63 can be taken to change from silicon to tissue (Bradley & Rosenfeld 2015).Considering a simple approach we have taken that the device capacitance depends linearly on the microdosimeter size parameter L while its leakage current varies linearly with the volume proportional to L^3. The behavior of microstructured silicon devices can be affected by other contributions not contemplated by the model. Nevertheless, this model helps to show the important outcome of the physical limitations for linear energy detection for non-intrinsic gain solid state devices.

If we take a standard approximation for the ENC (rms of the noise charge) of the charge sensitive amplifier, this would have a behavior

$$ENC = \sqrt{\frac{\alpha(C_{in}+\beta)^2}{\tau} + \gamma\tau(I_d+\delta) + \kappa}$$

whereas τ is the amplifier shaping time, C_{in} is the detector capacitance and I_d the

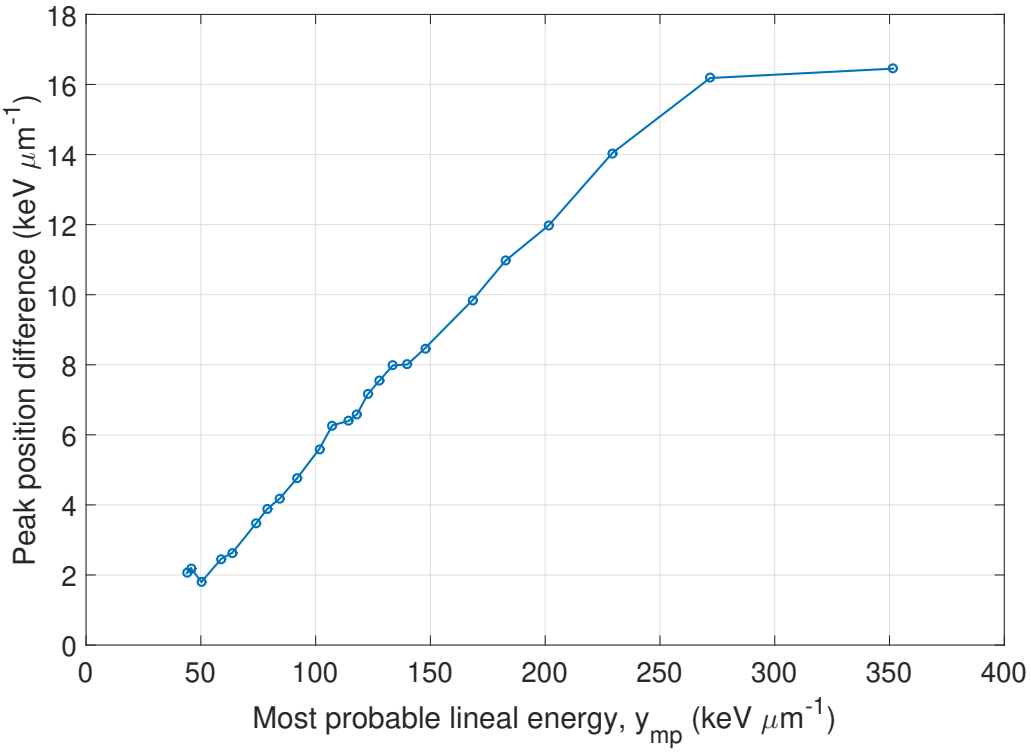

Figure 10. Peak shift in keV/μm for all measured points with the cylindrical microsensor along the Bragg curve as a function of the most probable lineal energy, y_{mp}.

detector leakage current and α, β, γ, δ and κ are noise parameters associated to the electronic readout chain due to shunt and series resistance, sensor bias current and amplifier contributions (Radeka 1974, Bertuccio & Pullia 1993). For this work, we have considered sizes L of cylindrical microdetectors from 0.1 μm up to 40 μm with C_{in} ranging from 0.01 pF up to 5.3 pF and I_d from 1 pA up to 950 pA. These values were taken according to our experience with similar devices. We used parameters from the state of the art electronics (*CR-110 reference sheet* n.d.) to calculate that ENC would yield values between 260 up to 290 electrons for a shaping time of 1 μs respectively ($\alpha = 43$ pF^{-2} μs e^2; $\beta = 15$ pF; $\gamma = 8$ μs^{-1} pA^{-1} e^2; $\delta = 800$ pA; $\kappa = 5 \times 10^4$ e^2). We have considered two scenarios, namely: when the track incidence is to be parallel to the cylinder axis considered above, thus having $< l >= L$ (denominated axial) and when there is μ-randomness with $< l >= \frac{2}{3}L$ (denominated isotropic). For the noise separation we have assumed that the $FWHM$ equivalent noise energy would be 2.35 times the ENC multiplied by the average energy w per ion-electron pair, thus providing a threshold on the energy imparted detection taken as two times this $FWHM$ (Radeka 1974)

$$\epsilon_{th} \geq 2 \times ENC \times 2.35 \times W$$

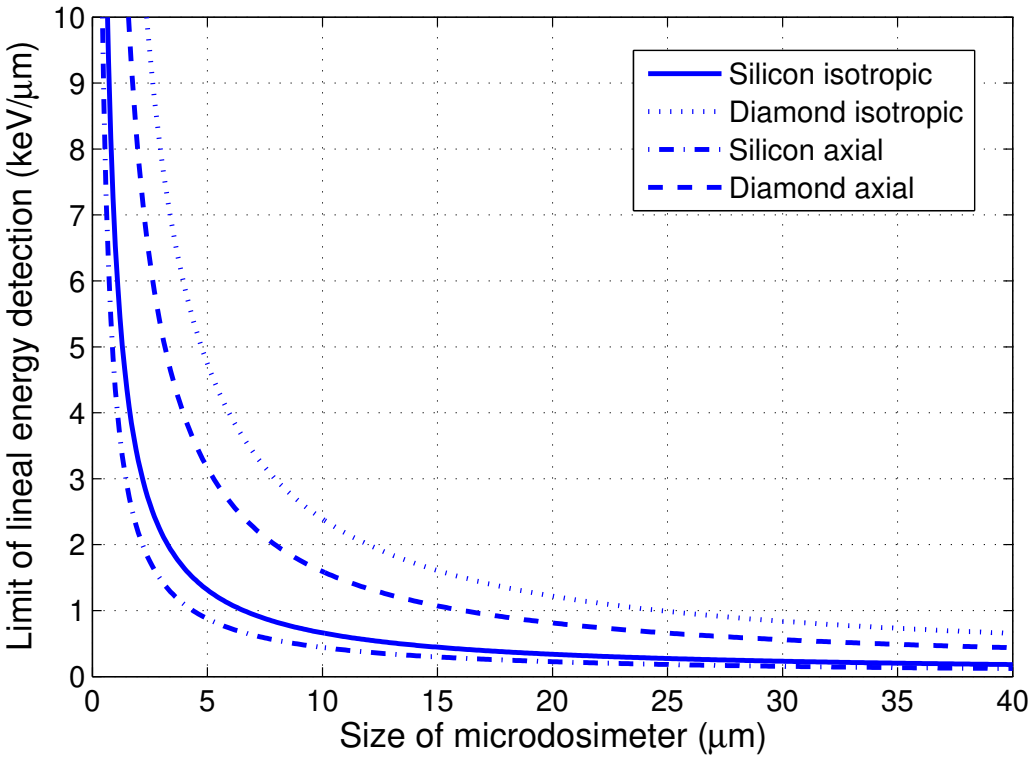

Figure 11. Limit of detectability for lineal energy in cylindrical micro–dosimeters with equal diameter and height L as a function of L. Dotted and continuous lines correspond to diamond and silicon detectors under isotropic conditions respectively. Dashed and dot-dashed lines correspond to diamond and silicon detectors for axial incidence respectively.

This provides also a corresponding limit on the lineal energy detection in the form of

$$y_{th} = \frac{\epsilon_{th}}{< l >} \geq \frac{4.7 \times ENC \times W}{< l >}$$

Thus we can evaluate the corresponding limits for the detection of the lineal energy considering these cylindrical microdetectors of different size L. Figure 11 shows the limits on the detection of lineal energy in the detecting material as a function of the detector size both for isotropic and parallel to the cylinder axis incidences. In this Figure we have included both diamond and silicon sensors just to guide the reader in terms of the physical limits expected from the different characteristics of the sensitive media.

In the axial incidence scenario, the capability to extend the detection range to 1 keV/μm would be achieved in silicon when the size of the microsensor is equal or bigger than 4.4 μm while in the case of diamond this would imply a sensor of 16 μm thickness. Additionally, it is clear that sub-micron microdosimeters would be only useful for highly ionizing particles, since for silicon (diamond) devices of 1 μm we would only be able to detect radiation with lineal energy over 4.5 keV/μm (15.7 keV/μm). This conclusion

tends to exclude the feasibility of solid state microdosimeters as adequate devices for track structure measurement in the region around 0.1 μm or below, at least for non intrinsic gain sensors. Those limits are even larger for the isotropic conditions where, for example, to achieve a detection limit below 1 keV/μm it would be needed a sensor of 6.7 μm size in silicon while for diamond this limit yields a value of 25 μm. In fact the use of devices of tenths of microns would yield values closer to the Linear Energy Transfer than the stochastic lineal energy considered in microdosimetric distributions. Of course, the results of this section could be recalculated considering the particular electronic noise, sensor characteristics and readout under study.

4. Conclusions

Solid-state devices can be employed to measure microdosimetric spectra. Charge collection efficiency (CCE) and electronic noise pose limitations on their performance since they can affect the fidelity of the microdosimetric distributions and the thresholds of lineal energy detection. For the cylindrical device studied in this work with 15 μm diameter and 5.5 μm thickness, the intrinsic field gradients and charge diffusion in the sensitive volume of the detector modify the recorded spectra by inducing a charge collection efficiency strongly dependent on the position of the energy deposition event. These perturbations modify the raw experimental microdosimetric spectra in a systematic way, producing an artificial enhancement of the low lineal energy region. In the present work this evidence was found in ^{12}C beam measurements at CNAO.

In order to reproduce this systematic effect we constructed a first phenomenological model for the CCE by using an exponential function and six parameters related to the physical dimensions of the microstructured detector. Electrical simulations using TCAD at different biasing voltages and proton beam IBIC tests performed to study the active volume inside the microdosimeters were additionally used to validate the CCE model.

Monte Carlo simulations were modified by using this model to compute the partial charge collection in the simulated energy deposition events. Reconstructed spectra including CCE effect showed considerable agreement with the experimental results. The most probable lineal energy in these experimental spectra is shifted with respect to the expectation value obtained with Monte Carlo simulations. This shift along the Bragg curve holds a linear relationship with the lineal energy.

Additionally to the distortion of the low lineal energy spectra, the electronic noise contribution sets a theoretical limit on the smallest detectable lineal energy for microstructured solid state devices. Considering a cylindrical device with equal diameter and height L, the lineal energy threshold would be inversely proportional to this parameter. For example, for detecting events of 1 keV/μm, the dimension L should be greater than 4.4 μm whereas in diamond this size should be at least 16 μm.

Acknowledgments

C Guardiola has received funding from the European Union's Horizon 2020 research and innovation program under the Marie Sklodowska-Curie grant agreement No 745109. M C Jiménez-Ramos acknowledge support from the Spanish project RTI2018-098117-B-C21 funded by Ministry of Science, Innovation and Universities.

References

Berger, M. J., Coursey, J., Zucker, M., Chang, J. et al. (1998). *Stopping-power and range tables for electrons, protons, and helium ions*, NIST Physics Laboratory Gaithersburg, MD.

Bertuccio, G. & Pullia, A. (1993). A method for the determination of the noise parameters in preamplifying systems for semiconductor radiation detectors, *Review of Scientific Instruments* **64**(11): 3294–3298.

Böhlen, T., Cerutti, F., Chin, M., Fassò, A., Ferrari, A., Ortega, P., Mairani, A., Sala, P. R., Smirnov, G. & Vlachoudis, V. (2014). The fluka code: developments and challenges for high energy and medical applications, *Nuclear data sheets* **120**: 211–214.

Böhlen, T. T., Cerutti, F., Dosanjh, M., Ferrari, A., Gudowska, I., Mairani, A. & Quesada, J. (2010). Benchmarking nuclear models of fluka and geant4 for carbon ion therapy, *Physics in Medicine & Biology* **55**(19): 5833–5847.

Bolst, D., Guatelli, S., Tran, L. T. & Rosenfeld, A. B. (2018). Optimisation of the design of soi microdosimeters for hadron therapy quality assurance, *Physics in Medicine & Biology* **63**(21): 215007.

Bradley, P. D. & Rosenfeld, A. B. (2015). Tissue equivalence correction for silicon microdosimetry detectors in boron neutron capture therapy, *Medical Physics* **25**(11): 2220–2225.

Brenner, D. & Ward, J. (1992). Constraints on energy deposition and target size of multiply damaged sites associated with dna double-strand breaks, *International journal of radiation biology* **61**(6): 737–748.

Britten, R. A., Peters, L. J. & Murray, D. (2001). Biological factors influencing the rbe of neutrons: implications for their past, present and future use in radiotherapy, *Radiation research* **156**(2): 125–135.

Campbell, M., Heijne, E., Holý, T., Idárraga, J., Jakubek, J., Lebel, C., Leroy, C., Llopart, X., Pospísil, S., Tlustos, L. & Vykydal, Z. (2008). Study of the charge sharing in a silicon pixel detector by means of α-particles interacting with a Medipix2 device, *Nuclear Instruments and Methods in Physics Research Section A: Accelerators, Spectrometers, Detectors and Associated Equipment* **591**(1): 38 – 41. Radiation Imaging Detectors 2007.

Colautti, P., Conte, V., Selva, A., Chiriotti, S., Pola, A., Bortot, D., Fazzi, A., Agosteo, S. & Ciocca, M. (2017). Microdosimetric study at the cnao active-scanning carbon-ion beam, *Radiation protection dosimetry* **180**(1-4): 157–161.

CR-110 reference sheet (n.d.). Accessed: 2019-06-03.

De Nardo, L., Cesari, V., Donà, G., Magrin, G., Colautti, P., Conte, V. & Tornielli, G. (2004). Mini-tepcs for radiation therapy, *Radiation protection dosimetry* **108**(4): 345–352.

Dosanjh, M., Amaldi, U., Mayer, R., Poetter, R. et al. (2018). Enlight: European network for light ion hadron therapy, *Radiotherapy and Oncology* **128**(1): 76–82.

Durante, M. & Loeffler, J. S. (2010). Charged particles in radiation oncology, *Nature reviews Clinical oncology* **7**(1): 37–43.

Farahmand, M., Bos, A., De Nardo, L. & Van Eijk, C. (2004). First microdosimetric measurements with a tepc based on a gem, *Radiation protection dosimetry* **110**(1-4): 839–843.

Ferrari, A., Sala, P., Fasso, A. & Ranft, J. (2005). "fluka: a multi-particle transport code", cern 2005-10 (2005), *Technical report*, INFN/TC_05/11, SLAC.

Fleta, C., Esteban, S., Baselga, M., Quirion, D., Pellegrini, G., Guardiola, C., Cortés-Giraldo, M., López, J. G., Ramos, M. J., Gómez, F. et al. (2015). 3d cylindrical silicon microdosimeters: fabrication, simulation and charge collection study, *Journal of Instrumentation* **10**(10): P10001.

Gimenez, E. N., Ballabriga, R., Campbell, M., Horswell, I., Llopart, X., Marchal, J., Sawhney, K. J. S., Tartoni, N. & Turecek, D. (2011). Study of charge-sharing in MEDIPIX3 using a micro-focused synchrotron beam, *Journal of Instrumentation* **6**(01): C01031–C01031.

Ginzberg, M. B., Kafri, R. & Kirschner, M. (2015). On being the right (cell) size, *Science* **348**(6236): 1245075.

Gómez, F., Fleta, C., Esteban, S., Quirion, D., Pellegrini, G., Lozano, M., Prezado, Y., Dos Santos, M., Guardiola, C., Montarou, G. et al. (2016). Measurement of carbon ion microdosimetric distributions with ultrathin 3d silicon diodes, *Physics in Medicine & Biology* **61**(11): 4036–4047.

Guardiola, C., Quirion, D., Pellegrini, G., Fleta, C., Esteban, S., Cortés-Giraldo, M., Gómez, F., Solberg, T., Carabe, A. & Lozano, M. (2015). Silicon-based three-dimensional microstructures for radiation dosimetry in hadrontherapy, *Applied Physics Letters* **107**(2): 023505.

IAEA (2008). Relative biological effectiveness in ion beam therapy (trs 461), *Technical report*, International Atomic Energy Agency.

Kliauga, P. (1990). Measurement of single event energy deposition spectra at 5 nm to 250 nm simulated site sizes, *Radiation Protection Dosimetry* **31**(1–4): 119–123.

Krämer, M. & Scholz, M. (2000). Treatment planning for heavy-ion radiotherapy: calculation and optimization of biologically effective dose, *Physics in Medicine & Biology* **45**(11): 3319.

Paganetti, H. (2014). Relative biological effectiveness (rbe) values for proton beam therapy. variations as a function of biological endpoint, dose, and linear energy transfer, *Physics in Medicine & Biology* **59**(22): R419.

Parker, S. I., Kenney, C. J. & Segal, J. (1997). 3d—a proposed new architecture for solid-state radiation detectors, *Nuclear Instruments and Methods in Physics Research Section A: Accelerators, Spectrometers, Detectors and Associated Equipment* **395**(3): 328–343.

Particle Therapy Co-Operative Group (2019). PTCOG home page.
URL: *https://www.ptcog.ch/*

Pellegrini, G., Fernández-Martínez, P., Baselga, M., Fleta, C., Flores, D., Greco, V., Hidalgo, S., Mandić, I., Kramberger, G., Quirion, D. et al. (2014). Technology developments and first measurements of low gain avalanche detectors (lgad) for high energy physics applications, *Nuclear Instruments and Methods in Physics Research Section A: Accelerators, Spectrometers, Detectors and Associated Equipment* **765**: 12–16.

Pellegrini, G., Garcia, F., Balbuena, J., Cabruja, E., Lozano, M., Orava, R. & Ullan, M. (2009). Fabrication and simulation of novel ultra-thin 3d silicon detectors, *Nuclear Instruments and Methods in Physics Research Section A: Accelerators, Spectrometers, Detectors and Associated Equipment* **604**(1-2): 115–118.

Pellegrini, G., Lozano, M., Ullan, M., Bates, R., Fleta, C. & Pennicard, D. (2008). First double-sided 3-d detectors fabricated at cnm-imb, *Nuclear Instruments and Methods in Physics Research Section A: Accelerators, Spectrometers, Detectors and Associated Equipment* **592**(1-2): 38–43.

Prieto-Pena, J., Gómez, F., Fleta, C., Guardiola, C., Pellegrini, G., Donetti, M., Giordanengo, S., González-Castaño, D. M. & Pardo-Montero, J. (2019). Microdosimetric spectra measurements on a clinical carbon beam at nominal therapeutic fluence rate with silicon cylindrical microdosimeters, *IEEE Transactions on Nuclear Science* **66**(7): 1840–1847.

Radeka, V. (1974). Signal, noise and resolution in position-sensitive detectors, *IEEE Transactions on Nuclear Science* **21**(1): 51–64.

Spieler, H. (2005). Semiconductor detector systems.